JACS
JOURNAL OF THE AMERICAN CHEMICAL SOCIETY
Article
pubs.acs.org/JACS

Formation, Migration, and Reactivity of Au–CO Complexes on Gold Surfaces

Jun Wang,[†] Monica McEntee,[‡] Wenjie Tang,[‡] Matthew Neurock,*[,‡] Arthur P. Baddorf,[†] Petro Maksymovych,*[,†] and John T. Yates, Jr.[‡]

[†]Center for Nanophase Materials Sciences, Oak Ridge National Laboratory, Oak Ridge, Tennessee 37831, United States
[‡]Departments of Chemical Engineering and Chemistry, University of Virginia, Charlottesville, Virginia 22904, United States

Supporting Information

ABSTRACT: We report experimental as well as theoretical evidence that suggests Au–CO complex formation upon the exposure of CO to active sites (step edges and threading dislocations) on a Au(111) surface. Room-temperature scanning tunneling microscopy (STM), X-ray photoelectron spectroscopy, transmission infrared spectroscopy, and density functional theory calculations point to Au–CO complex formation and migration. Room-temperature STM of the Au(111) surface at CO pressures in the range from 10^{-8} to 10^{-4} Torr (dosage up to 10^6 langmuir) indicates Au atom extraction from dislocation sites of the herringbone reconstruction, mobile Au–CO complex formation and diffusion, and Au adatom cluster formation on both elbows and step edges on the Au surface. The formation and mobility of the Au–CO complex result from the reduced Au–Au bonding at elbows and step edges leading to stronger Au–CO bonding and to the formation of a more positively charged CO ($CO^{\delta+}$) on Au. Our studies indicate that the mobile Au–CO complex is involved in the Au nanoparticle formation and reactivity, and that the positive charge on CO increases due to the stronger adsorption of CO at Au sites with lower coordination numbers.

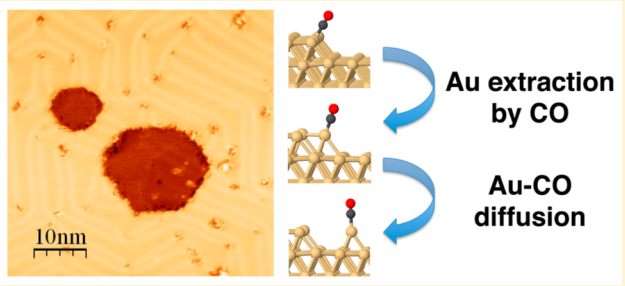

I. INTRODUCTION

The unique catalytic activity of gold nanoparticles is of increasing interest due to their application in the partial oxidation of a range of different molecules, including CO, H_2, C_2H_4, acetic acid, and fatty acids.[1−7] Haruta et al. were the first to discover and demonstrate the unusually high catalytic activity for nanometer-sized Au particles supported on metal oxides for CO oxidation at temperatures lower than 273 K.[8] Numerous experimental and theoretical studies followed the pioneering work of Haruta and have helped to elucidate the nature as well as the location of the active sites and provide direct insights into the mechanisms that control oxidation. The catalytically active sites are thought to reside at the perimeter of the ∼3 nm diameter Au nanoparticles supported on TiO_2.[6,9−11] These sites are able to dissociate O_2 with activation energies of ∼0.5 eV. Molecular oxygen is thought to initially adsorb at Au–Ti^{4+} ion site pairs at Au perimeter sites and form Ti–O–O–Au peroxo-like intermediates that can readily activate CO at the periphery of the Au/TiO_2 interface.[6] CO oxidation preferentially occurs at these perimeter Au–Ti^{4+} sites as they demonstrate the lowest activation energies of all of the sites examined.[6] Rodriguez et al. synthesized inverted Au catalysts comprised of TiO_2 nanoparticles on a Au(111) single crystal to provide strong evidence that further supports the role of perimeter sites at the Au/TiO_2 interface for catalyzing the water gas shift reaction.[12] Hutchings et al. extended these ideas by synthesizing monolayer and bilayer Au clusters comprised of an abundance of low-coordinated Au sites, supported on a metal oxide support, and demonstrated significant increases in the CO oxidation reactivity on the smaller Au nanoparticles.[13]

Early theoretical studies were carried out to demonstrate the importance of coordinatively unsaturated Au sites and Au sites present at the perimeter of the oxide support in the oxidation of CO. Hammer and Nørskov reported significantly stronger binding energies for CO and O_2 molecules at the Au perimeter sites and lower CO oxidation barriers than those bound to the more coordinatively saturated Au top sites.[14,15] Landman et al. examined IR frequency shifts for CO on Au_8 clusters supported on MgO and showed a characteristic red shift in the CO frequency for CO on the Au_8 cluster supported on the defect free MgO support as compared to CO on Au_8 bound to a defect site on the MgO support.[16] The charge transfer from the defect to the Au particle and then to the CO molecule changed not only the frequency but also the reactivity of the CO. Others have come to similar conclusions and report that[17−19] (1) low coordination Au sites are reactive toward CO oxidation, and (2) changes in the electronic properties play an important role in CO adsorption and reactivity.

In addition to the Au atoms that reside at the Au/metal oxides interface, other Au sites on the Au particle surface can also catalyze CO oxidation, particularly the Au atoms at step

Received: August 28, 2015
Published: January 12, 2016

DOI: 10.1021/jacs.5b09052
J. Am. Chem. Soc. 2016, 138, 1518−1526

and kink sites, which exhibit lower Au coordination numbers and increased CO adsorption energies.[1,3] CO oxidation at these Au sites has been observed at temperatures at ~300 K by using IR spectroscopy, which can directly observe the oxidative consumption of chemisorbed CO on the Au surface.[1,3]

Previous studies have shown that strongly bound adsorbates often result in weaker metal−metal bonds and generate mobile metal−adsorbate complexes.[20−24] Direct evidence on the formation of CO−Pd complexes was found for Pd adatoms supported on a Fe_3O_4 surface,[25] and the important role of CO on the mobility and sintering for these CO−metal complexes was elucidated.[25,26] In a recent theoretical paper,[27] Rousseau et al. postulated that CO molecules bound to Au migrate not as individual CO molecules, but as a triatomic Au−CO complex. This would suggest the migration of Au−CO complexes with weaker Au−Au bonding and would be consistent with a number of other systems where adsorbate bonding generates mobile metal−adsorbated complexes,[20−24] or even organometallic structures on the surface of gold.[24] An important question therefore is whether the CO that is present on the Au surface of the Au nanoparticle interacts with the gold lattice to create intermediate organometallic Au−CO_x complexes.

A previous surface X-ray diffraction study provided evidence of CO reacting with the Au(111) surface by lifting the Au(111) reconstruction at elevated pressures.[28] Piccolo et al. showed CO modified the Au(111) surface by lifting the herringbone reconstruction at an elevated CO pressure ($P_{CO} \geq 250$ Torr).[29] The same group also showed CO could chemisorb on Au(110) and modify the Au(110) surface by forming Au−CO species under high CO pressures of 0.1−100 Torr[30] and presented first-principle theoretical results that suggest the formation of Au−CO entities on Au(110) at high CO pressures.[31] Furthermore, several spectroscopic studies of the CO reactivity on Au/TiO_2 also speculated the possible modification and rearrangement of Au nanoparticles under elevated CO pressure.[32,33] Hrbek et al. used scanning tunneling microscopy along with infrared absorption spectroscopy to show the adsorption of CO at the edges of hexagonal vacancies of Au(111) surface at cryogenic temperature and its role in restructuring of Au resulting in the rounding of Au edges and the formation of nanometer-sized Au particles.[34] Their theoretical results support the formation of a Au-CO complex at the coordinatively unsaturated Au sites and its facile diffusion. It was subsequently reported that high pressure CO causes smoothing of the sputtered roughened Au(111) surface by CO-facilitated reordering of the Au surface.[35] A more complete understanding of the Au−CO interaction and the mobility of this Au−CO complex is therefore needed to understand the surface chemistry. Although the postulation of a Au−CO complex is suggested as the mobile intermediate, the detailed mechanism and kinetics for the formation and migration of such a Au−CO complex is still missing.

In this work, we report a comprehensive study of CO interactions and reactivity on nanostructured Au(111) and present high-resolution scanning tunneling microscopy (STM), X-ray photoelectron spectroscopy (XPS), transmission infrared (IR) spectroscopy, and density function theory (DFT) calculations that suggest the early stage evolution of Au−CO species formation and migration on Au(111) surfaces subjected to CO pressures ranging from high vacuum (10^{-8} Torr) to moderate vacuum (10^{-4} Torr) at room temperature. A nanostructured Au(111) surface with hexagonal shaped nanopits with monatomic depth was prepared to increase lower coordination Au sites. We find that CO strongly interacts with the Au(111) surface and initiates the likely formation of Au_x−CO complexes at both the step edges and the herringbone reconstruction elbow (strain) sites. The Au_x−CO complexes subsequently detach, diffuse, and add to growing Au islands. The process is thought to proceed by (1) the adsorption and interaction of CO on Au sites at step edges produced by edge roughing and elbow sites of the gold herringbone reconstruction; (2) extraction and excessive ejection of Au atoms on the elbow and step edges; and (3) growth of Au into larger ad-islands, which cover more area on the gold surface. By combining the results from transmission IR spectroscopy, CO adsorption measurements on Au, and DFT simulations of Au-etch pit erosion by CO, we gain detailed insights into the formation and migration of mobile Au−CO complexes.

II. EXPERIMENTAL SECTION

The STM experiments were conducted by using an internally designed variable temperature scanning tunneling microscope in an ultrahigh vacuum (UHV) chamber with a base pressure of 1×10^{-10} Torr. The Au(111) sample was cleaned via a standard sputtering and annealing process. Hexagonal nanopits on Au(111) were created by briefly sputtering the heated (~423 K) Au sample with Ar^+ ions (1 kV, 1.0×10^{-7} Torr, for 1 min). A commercial Pt−Ir STM tip was prepared by gentle field emission treatments on a clean gold surface. The bias voltage was applied on the Au(111) sample. STM images were taken at room temperature, as our previous low-temperature STM studies did not show CO reactivity with Au(111) at 5−40 K[36] probably due to the presence of an activation barrier for Au−CO complex formation and mobility that cannot be overcome at these low temperatures. The research grade CO (ultrahigh purity) gas was purchased from Matheson. To eliminate the possible iron carbonyl impurity, we cooled CO with liquid nitrogen (LN2) using a laboratory-built cryotrap line immersed in a LN2 dewar before CO was admitted into the UHV chamber. This way, CO was condensed at 77 K and the actual admitted CO gas was from the equilibrium CO vapor pressure of ~0.4 bar (300 Torr). After we established Au ad-island formation on the surface following the final CO dose, we transferred the sample to an XPS equipped chamber to confirm that the ad-island features were indeed gold clusters. A monochromated Al Kα source (SPECS FOCUS 500) and a hemispherical electron energy analyzer (SPECS Phoibos 150) were used.

A high vacuum chamber was used to carry out the IR experiments with a base pressure of $\sim 1 \times 10^{-8}$ Torr. The experimental design was described in detail elsewhere.[1,3] The Au/TiO_2 and Au/SiO_2 catalysts were synthesized by the precipitation−deposition method provided by Zanella et al., with the Au/SiO_2 sample given to us already synthesized by Zanella.[37,38] Detailed characterization indicated that both IR-studied catalysts were comprised of ~3 nm diameter Au particles. The 3 nm Au particles are assumed to exhibit reduced Au−Au bonding on the particle surface because of the high degree of curvature. CO (99.9% purity, Matheson) was further purified using a LN2 trap attached to the vacuum gas line similar to the STM setup described above.

First principle density functional theory (DFT) calculations were carried out to gain insights into the bonding of CO on Au and the correlation between the CO frequency on Au sites and the Au coordination numbers (CN) for the CO adsorption sites. The pitted Au(111) surface was simulated using a (5 × 3) slab with 4 atomic layers and a step (Figure 1a) as well as an elbow (Figure 1b) present along the edge of an upper Au(111) terrace. The step sites and elbow sites were chosen to directly mimic the reactive edge and elbow sites for Au−CO formation and extraction on the Au(111) surfaces. The bottom two layers in the simulations were fixed to the Au lattice positions.

All of the DFT calculations reported herein were carried out using the Vienna Ab Initio Software Package (VASP)[39] program with plane-wave basis sets and cutoff energies of 400 eV. The core electrons were

DOI: 10.1021/jacs.5b09052
J. Am. Chem. Soc. 2016, 138, 1518−1526

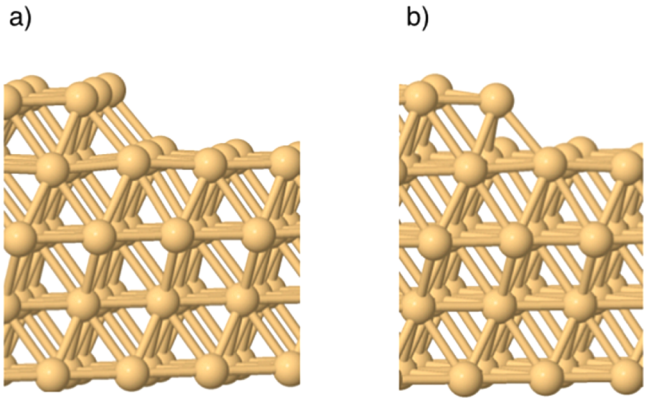

Figure 1. Side view of the computational models for (a) a Au(111) step edge to mimic the side of a pitted Au(111) surface, and (b) the elbow site.

treated by pesudopotentials with the projector augmented-wave (PAW) method.[40,41] The revised Perdew–Burke–Ernzerhof (PBE) form of the gradient approximation (GGA) functional was used to model the exchange-correlation effects.[42] Spin-polarization was tested for CO adsorbed at different sites on the Au step edge model of the side of a pitted Au surface. The results show very similar binding energies (<2 kJ/mol) and thus very little influence of spin-polarization. The Au(111) slab was simulated with a (2 × 1 × 1) *k*-point mesh[43] with a 15 Å vacuum gap in the *z*-direction. Geometries were considered optimized when the forces on each atom were less than 0.03 eV/Å. The calculated vibrational frequencies have been scaled by a factor of 1.02, which is the ratio between the measured (2143 cm^{-1}) and calculated (2102 cm^{-1}) stretch frequencies for gas-phase CO. The charge associated with each atom was subsequently calculated using the Bader analysis.[44,45]

III. RESULTS AND DISCUSSION

3.1. STM. Artificially created hexagonal shaped pits with monatomic depth on Au(111) were generated by gentle Ar^+ sputtering (1 kV, 1.0 × 10^{-7} Torr, for 1 min) on a slightly heated sample. The resulting structure of these surfaces is captured in Figure 2. The six atomic steps in each pit were located along the close-packed directions of Au(111), and the hexagonal shape was the most stable structure thermodynamically. The average length of these step edges ranged from 5 to 20 nm. The generation of these pits provided an abundant number of low coordination number Au sites on these step edges that should facilitate the postulated formation of the Au–CO complex.

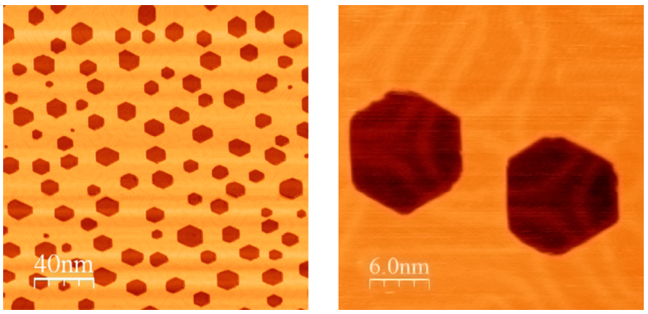

Figure 2. Left panel: A typical Au(111) surface after a gentle sputtering shows atomically clean, hexagonal shaped pits with monatomic-depth and sharp edges (sample bias U = 1 V, current I = 30 pA). Right panel: A magnified STM image shows only two monatomic hexagonal pits on Au(111) with a herringbone reconstruction pattern visible (U = 3 mV, I = 50 pA).

A precooled purified CO gas was introduced into the chamber (and onto the surface) in the procedure discussed earlier in the Experimental Section. The sharp edge of the pits that evolved gradually due to the roughness and erosion is presented in Figures 3–5.

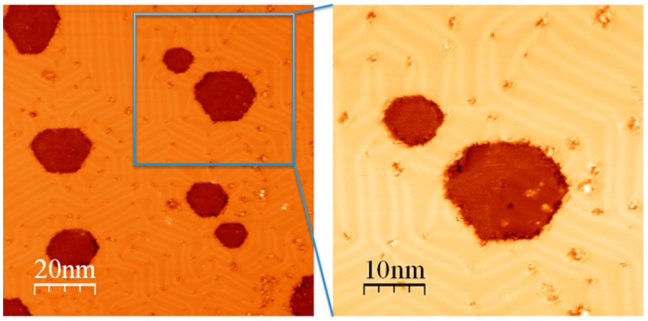

Figure 3. STM images taken (U = 0.6 V, I = 80 pA) after several CO exposures on pitted Au(111) (total ~5.5 h), from 4.0 × 10^{-8} to 1.6 × 10^{-6} Torr, with a total CO dose of ~1.3 × 10^4 langmuir. Missing atoms occur primarily on the soliton and within the FCC elbow of the gold herringbone reconstruction; the edges of the pits are also eroded.

The surface topography of the pitted Au(111) substrate after a total CO dose of ~1.3 × 10^4 langmuir (dose range from 4.0 × 10^{-8} to 1.6 × 10^{-6} Torr with a total dose time of 5.5 h) in Figure 3 shows an increase in roughness at the edges of pits. These rough structures subsequently evolve toward a more rounded shape. The other observation is that missing atoms occur over the surface, and the primary sites of missing atoms are at misfit dislocations (so-called elbow sites) of the gold herringbone reconstruction. These gold sites are similar to the strained Au sites at step edges that are considered responsible for the activation of CO.[46] Both step edge and elbow sites are seen in our high-resolution STM images. Although the overall hexagonal shape of pits did not change significantly, the steps decorating the pits became noticeably serrated. This agrees with Hrbek's work at cryogenic temperature,[34] which formed a beautiful prequel to our efforts here carried out at 300K and at saturate coverage. We note, however, that the steps and elbows are not generally sites with identical activity. This is consistent with the earlier work of Kim et al. in their infrared reflection–absorption spectroscopy (IRAS) measurement for CO on stepped Au(211) vicinal surfaces.[47] They determined that the first Au sites to be populated by CO were step sites, followed by terrace sites as the CO coverage increased; here, the ν(CO) red-shifted from 2126 cm^{-1} (low CO coverage) to 2112 cm^{-1} (high coverage).[47] Also, Piccolo et al. calculated the CO adsorption energy on various Au surface configurations and predicted the favorable adsorption trend for CO on Au was in the increasing order of adatoms > kinks > steps > terraces.[29] Thus, the maximum Au–Au coordination near an adsorbed CO molecule leads to the weakest CO binding energy and the lowest ν(CO) frequency.

The STM images of pitted Au(111) after a CO dose of 1.0 × 10^{-4} Torr for ~62 min, which is about 3.7 × 10^5 langmuir, presented in Figure 4 show that distinct clusters start to nucleate on both step edges and elbow sites primarily located in the FCC domain of the herringbone structure. These clusters noticeably appear in the consistent elbow positions where the

DOI: 10.1021/jacs.5b09052
J. Am. Chem. Soc. 2016, 138, 1518–1526

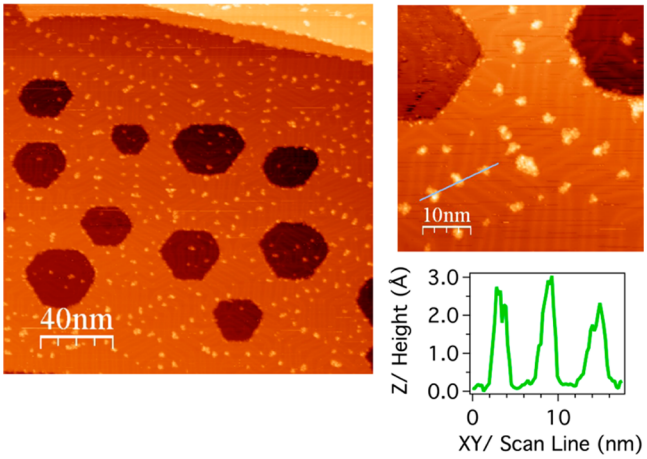

Figure 4. STM images (U = 0.8 V, I = 80 pA) of pitted Au(111) after CO dose at 1.0 × 10^{-4} Torr for ∼62 min (3.7 × 10^5 langmuir). Clusters start to nucleate on both step edges and elbow sites primarily located in the FCC domain of the herringbone. The line profile indicates the average size of the clusters is ∼5 nm, and the height of the clusters is about one Au atom.

holes are located in Figure 3. One possible explanation for the occurrence of these clusters is that the surface first undergoes the creation of holes by extracting surface gold atoms. The mobile CO−Au adatom clusters subsequently diffuse into both the hole as well as the step sites, and finally accumulate enough to form Au clusters. Loffreda et al. predicted that the extraction energy for Au−CO (0.85 eV) from the Au(110) surface was smaller than the direct extraction of a bare Au atom (1.28 eV) from the Au(110) but found that their diffusion energies were both about ∼0.5 eV.[31] These results indicate that the Au−CO complex is easier to extract than a Au atom alone. However, in the time frame of STM image taking, CO is already gone as it desorbs at 300 K. Defects and step edges comprised of coordinatively unsaturated Au atoms result in the strongest adsorption sites for these Au clusters. This explains why the CO−Au adatom interaction produces some nucleation at elbows, while the pure Au-adatom dynamics do not. The line profile in Figure 4 is an example that depicts the size of these clusters. The average cluster size is about 5 nm, and it is about one atom height of Au. One should notice that the size of clusters is larger than the holes; this is because the mobile gold complexes originate from both elbow (strained) sites and high-density step edges. Our observation provides details on CO extracting Au atoms from herringbone elbows and the initial formation of the Au−CO complex that Piccolo and co-worker's early STM work implied.[29,30] They showed the Au clusters on step edges and completed herringbone lifting at elevated CO pressure (100−250 Torr) on Au(111); they also showed that Au−CO species formed on a much more reactive Au(110) surface.

An extra dose of CO at 5.0 × 10^{-4} Torr for 122 min was given in addition to the dosage of 1.0 × 10^{-4} Torr for ∼62 min reported in Figure 4, for a total CO dose of about 4.0 × 10^6 langmuir, to further examine the influence of CO dosage on the Au surface structure. The results reported in Figure 5 show that the average cluster size increases from 5 nm (Figure 4) for the dosage of 3.7 × 10^5 langmuir CO to 10 nm average for the 4.0 × 10^6 langmuir dosage, while the height remains at about one atom of Au. This implies that more Au atoms are pulled out of the surface at higher dosages of CO and continue to accumulate into existing clusters at the low coordinate Au step sites and strained elbow sites. The herringbone reconstruction is still not completely lifted at this CO dosage, as we can vaguely see some soliton lines in the high-resolution STM images in Figure 5.

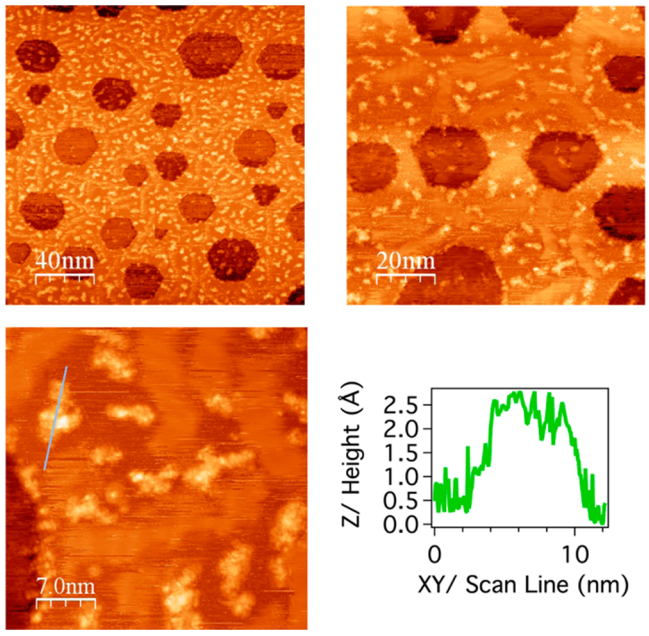

Figure 5. STM images (U = 0.8 V, I = 80 pA) of Au(111), after a total CO dose of about 4.0 × 10^6 langmuir. The line profile indicates that the average cluster size (∼10 nm) nearly doubles as compared to the cluster size reported for the lower CO dose (3.7 × 10^5 langmuir) experiments reported in Figure 4.

However, if the adatom clusters still reside on the elbow sites, their periodicity is clearly disrupted as compared to the clean Au(111) surface; that is, the herringbone reconstruction is now at least partially lifted.

On the basis of these observations, we quantified the density of Au−CO clusters and approximate coverage of presumed Au−CO complexes as a function of CO dosage in Figure 6. It is clear that the overall number and coverage of the presumed Au−CO complexes increase as a function of CO dosage (the blue curve). Furthermore, most of the initial clusters form at the elbow sites of the herringbone reconstruction (compare red and green curves). However, past ∼400 000 L, the number of visible clusters starts to decrease (while their size increases), which indicates early stages of the lifting of the herringbone reconstruction. By itself, lifting of the reconstruction directly points to adatom harvesting from the gold surface, as was earlier shown for alkanethiols.[24] However, it is clear that the predominant source of the adatoms in our case must be the step edges.[24]

To rule out any other possible impurities for these observed clusters, we subsequently transferred the sample directly into an XPS chamber to analyze the elemental composition of the clusters. The results from the XPS spectrum reported in Figure 7 show small C and O peaks that are expected as a result of exposure to air during the sample transfer as well as a fairly small peak for Zn (∼0.7%); no other impurities were observed. The Zn percentage was estimated by comparing the ratio of (relative peak intensity in Figure 6)/(sensitivity factor) between Zn $2p_{3/2}$ (sensitivity factor 18.91) and Au $4f_{7/2}$ (sensitivity factor 9.58), which results in a percentage =

DOI: 10.1021/jacs.5b09052
J. Am. Chem. Soc. 2016, 138, 1518−1526

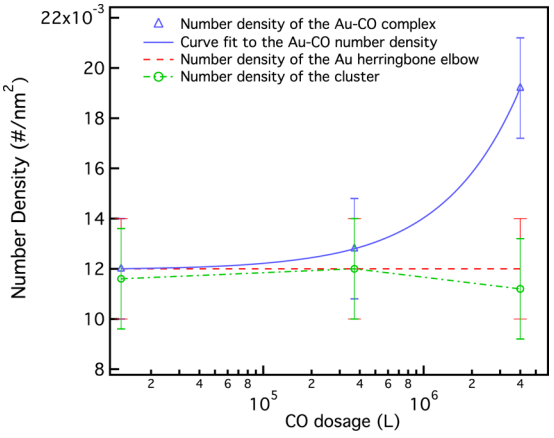

Figure 6. Changes in the number density of adatoms and defects as a function of CO dosage. Blue solid curve represents the estimated number density for the supposed Au−CO complex. Green dashed curve depicts the number density of the Au−CO cluster. Red dashed line represents the number density of the Au(111) herringbone elbow site on the pristine surface. The error bars were estimated as 0.002 #/nm^2 for the number density.

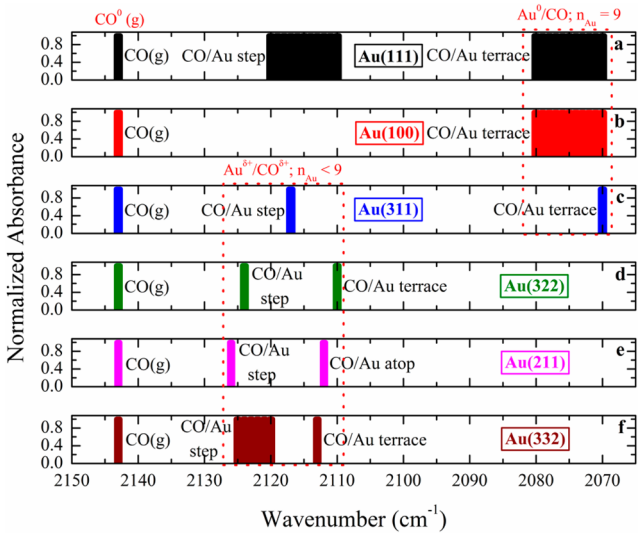

Figure 8. General differences in ν(CO) for CO adsorbed on smooth high-Au coordinate surfaces and Au surfaces with sites that have lower Au coordination numbers (n_{Au-Au}).

(32.7−28.7)/(18.91):(280−6)/(9.58) = 0.007:1 = 0.7%. This randomly observed 0.7% Zn impurity was probably from the valve adapter of the gas cylinder. It was unlikely associated with these STM observed ad-clusters on Au(111) and likely did not affect their mobility, because a conservative estimate for the surface rate of these clusters was well above 11.0% at the corresponding CO dosage in Figure 5.

3.2. IR Spectroscopy of CO Chemisorption on Au Surfaces. The IR studies of the CO stretching frequency (ν(CO)) directly reveal the distinct modification of the molecule when it is bound to the low-coordinated sites. Figure 8 compares different vibrational spectra for CO based on the literature data.[29,35,47−50] There is a 1.8% increase in ν(CO) in moving from CO on the Au terrace sites on the Au(111) surface to CO bound to lower coordinate Au sites (Figure 8). Three phenomena are present that might lead to this increase in ν(CO): (1) reduction in the number of Au−Au coordination sites (n_{Au-Au}); (2) transfer of electrons from CO to Au as n_{Au-Au} decreases, resulting in an increase in ν(CO) as $CO^{\delta+}$ forms; and (3) enhancement of CO bonding to nearby Au sites as n_{Au-Au} decreases. The influence of these three effects on the electronic structure is evaluated by DFT methods in section 3.3.

The IR spectra reported here show that low coordinated Au sites, which are observed by STM to migrate after CO adsorption, are abundant on Au nanoparticles and likely diffuse as CO−Au complexes on Au nanoparticle catalysts. We have independently carried out IR measurements for CO adsorption studies on supported Au nanoparticles. TiO_2 and SiO_2 surfaces were chosen as oxide supports to ensure that the differences in

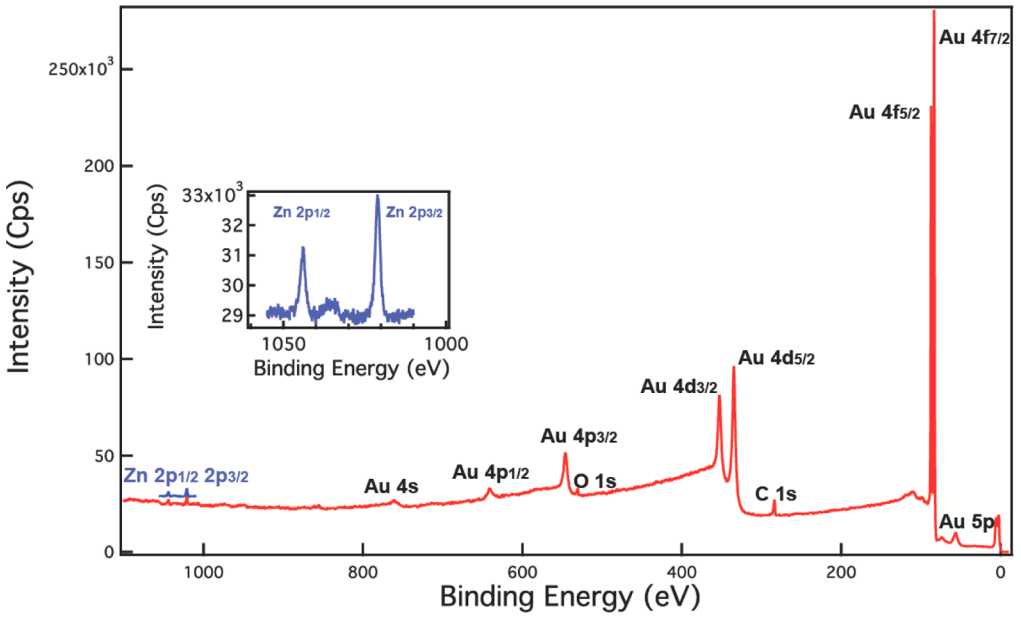

Figure 7. XPS spectrum for the Au(111) sample after a total CO dosage of about 4.0 × 10^6 langmuir as was reported in Figure 5. The red spectrum is a complete survey on the sample, while the blue one is the spectrum over the possible Zn impurity; the inserted spectrum is a zoom-in view for Zn.

DOI: 10.1021/jacs.5b09052
J. Am. Chem. Soc. 2016, 138, 1518−1526

ν(CO) are not the result of electronic differences between the semiconducting TiO_2 and the insulating SiO_2 supports. The results reported in Figure 9 show that the ν(CO) is very similar

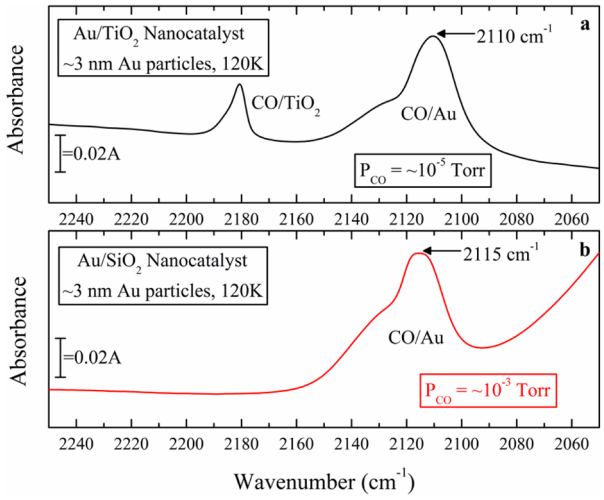

Figure 9. Infrared absorption spectra for CO adsorption on ~3 nm Au particles on (a) TiO_2 at 10^{-5} Torr of CO and (b) SiO_2 at ~10^{-3} Torr of CO. The similar spectra suggest that the n_{Au-Au} coordination sites are similar for Au on both oxide surfaces.

for ~3 nm diameter Au particles on both supports, thus indicating that the Au−Au coordination issue is not strongly related to the electronic character of the two oxides. The CO−Au blue-shifted IR wavenumbers shown as shoulders (2120−2140 cm^{-1}) in Figure 9 are due to the low-coordinated Au perimeter sites bonded to O atoms in the TiO_2 and SiO_2 supports, which extract electron density from the Au sites to the electronegative O atoms causing larger blue-shifts in the IR frequencies.

3.3. Density Functional Theory Calculated Changes in the Adsorption Energies and Vibrational Properties for CO at Different Au Sites on Model Au Surfaces and Particles. The changes in the overall energies and activation barriers for the formation and extraction of the Au−CO complex at the top of the step edge and the diffusion of the Au−CO complex from the top of the step down onto the Au(111) surface (with Au coordination numbers of 7) are shown in Figure 10a (as a function of CO coverage). The CO that adsorbs at sites along the top of the step edge can extract the corresponding Au atom from the edge to form a Au−CO complex that binds to the stable 4-fold Au site along the Au step edge (shown in the center of Figure 10a). The Au−CO complex subsequently diffuses down onto and along the terrace to coordinate to three Au atoms on the Au(111) surface (shown on the far right of Figure 10a). At low CO coverages on the edge sites (1/3 of the Au atoms), the adsorption energy was calculated to be −0.54 eV, whereas the activation barriers for Au−CO extraction and Au−CO diffusion were calculated to be 0.62 and 0.38 eV, respectively. These barriers are significantly lower than the barriers of 0.80 and 0.46 eV calculated for the direct detachment of a Au atom from the step edge and Au atom diffusion on the unreconstructed Au(111) surface, respectively. The barriers calculated here for Au−CO extraction and Au−CO diffusion are accessible at 300 K even with conservative estimates of kinetic pre-exponential factors. The CO−Au complexes that form can subsequently diffuse and

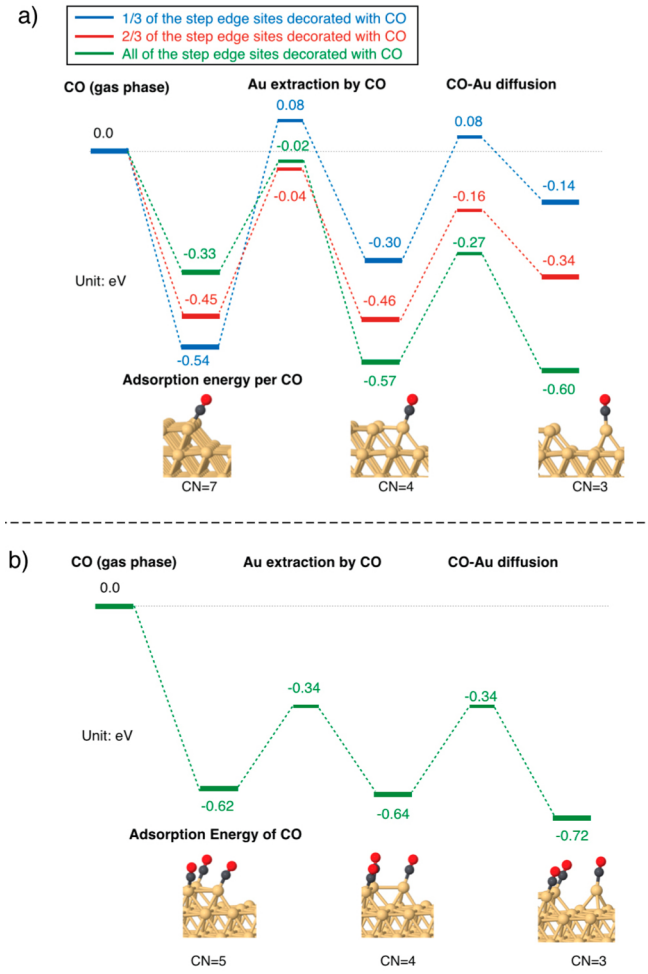

Figure 10. Reaction energy diagram for (a) CO−Au extraction from an atomic step edge of Au and the subsequent diffusion barrier for the migration of Au−CO from the step to the (111) terrace surface as a function of the coverage of CO along the Au edges. The blue, red, and green curves refer to surfaces where 1/3, 2/3, and 1 of the total Au edge sites are covered in CO. (b) CO−Au extraction from an elbow site along an edge of a (111) island, which was calculated to be 0.28 and 0.30 eV, respectively.

combine with other Au atoms, Au−CO complexes, or Au clusters to form larger Au clusters on the surface. The number of bonds between the Au−CO complex and the Au surface decreases from 7 to 4 to 3 as the Au−CO complex is formed at the top of the step, diffuses down along the step edge and onto the Au(111) terrace, and diffuses away from the step edge along the Au(111) surface.

The barriers reported above assumed that the CO coverage on the surface was rather low (where only 1/3 of the Au edge sites are occupied with CO). The edge sites that are coordinatively unsaturated are likely to adsorb more CO and as such have higher CO coverages. The adsorption energies increased from −0.54 to −0.45 and −0.33 eV (become weaker), whereas the barriers for CO−Au extraction decreased from 0.62 to 0.41 and 0.31 eV and the barriers for CO−Au diffusion decreased from 0.38 to 0.30 and 0.30 eV as the CO coverage of the edge sites increased from 1/3 to 2/3 and 1, respectively. The results clearly show an increase in the formation and mobility at the higher CO coverage along with an overall increase in the favorability of Au−CO formation, extraction, and diffusion. Similar behavior was also found for

DOI: 10.1021/jacs.5b09052
J. Am. Chem. Soc. 2016, 138, 1518−1526

the CO bound to the elbow sites at full CO coverages where the barriers for Au−CO formation and diffusion were calculated to be 0.28 and 0.3 eV, respectively, as is shown in Figure 10b: the coordination number of the Au decreases from 5 to 4 to 3 during the Au−CO complex extraction and diffusion process.

The changes that occur in the Au coordination ultimately result in shifts in the CO stretching frequency (ν(CO)). A decrease in the coordination number of the adsorption site results in the formation of a stronger binding of CO to Au, a more positive charge on the CO, and higher ν(CO), as can be seen in the results reported in Figure 11. After the extraction of

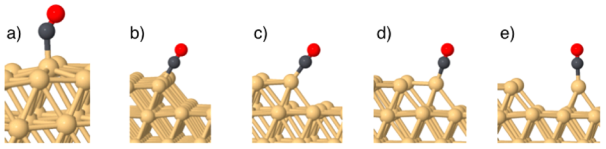

Site	CN	d(C-O) (Å)	d(Au-C) (Å)	v(CO) (cm^{-1})	Charge on CO	CO binding energy (eV)
a	9	1.15	2.13	2061	0.00 e	-0.04
b	7	1.15	1.97	2081	+0.02 e	-0.54
c	5	1.16	1.96	2087	+0.03 e	-0.65
d	4	1.16	1.96	2091	+0.03 e	-0.72
e	3	1.16	1.94	2094	+0.04 e	-0.86

Figure 11. DFT-calculated CO and Au−C bond lengths, CO−Au adsorption energies, ν(CO), and charges on CO for Au sites with coordination numbers of 3, 4, 5, 7, and 9.

the CO−Au complex, the step edge exposes Au sites with lower CN (CN = 6). CO adsorption can quickly take place at these unsaturated Au sites and facilitate Au−CO diffusion and initiate subsequent Au−CO extraction steps.

To better understand the shifts in ν(CO) with Au coordination number, we systematically examined the adsorption of CO at different sites on the monatomic-high Au structure. We calculated the Au−CO bond length, CO adsorption energy, ν(CO), and the charge on CO for Au sites with coordination numbers of 3, 4, 7, and 9 on the monolayer Au structure on Au(111), as shown in Figure 11. CO weakly binds to the coordinatively saturated Au sites, which have CN = 9, resulting in an adsorption energy of −0.04 eV that is in good agreement with the weak adsorption of CO on Au(111) reported by others.[51−53] The adsorption of CO becomes significantly stronger as the coordination of the Au sites decreases. The calculated CO adsorption energies decrease (become stronger) from −0.54, −0.65, −0.72, and −0.86 eV as the CN of the Au sites decreases from 9 to 7, 5, 4, and 3. The calculated CO frequency shifts to higher wavenumbers as the CN of the Au adsorption site decreases, from 2061 cm^{-1} on a CN = 9 Au site to 2081, 2087, 2091, and 2094 cm^{-1} on Au sites with coordination numbers of 7, 5, 4, and 3, respectively. The stronger adsorption energies with reduction of the coordination number are consistent with previous findings reported in the literature.[31,34,51−55] These changes are also consistent with results reported in Figure 11, which show a decrease in the Au−C bond length and an increase in the C−O bond length as the Au CN is decreased from 9 to 3.

The results reported in Figure 11 indicate that the ν(CO) shifts are correlated with the charge on CO. The charge on the CO at the more coordinatively saturated Au sites (CN = 9) is neutral, while the charge on the CO at the less-coordinatively saturated Au sites becomes more positive, resulting in charges of +0.02 e for CN = 7, +0.03 e for CN = 4 and 5, and +0.04 e for CN = 3. The adsorbed CO donates more electrons to the Au as the CN on the Au decreases, thus resulting in more positive charge on CO itself. The increase in the positive charge on CO shifts the ν(CO) to higher wavenumbers. As such, CO molecules bound to the low CN sites result in higher frequencies than those CO molecules adsorbed at high CN sites.[51−53] While the changes in charge reported here are small, they show a linear increase with increasing positive charge on CO. This is consistent with previous experimental and theoretical results, which showed that increasing the positive charge CO (increasing negative charge on Au) via the adsorption of charge donors onto the TiO_2 support increased the CO stretching frequency.[7]

In addition to the Au coordination number, the coverage of CO on the surface can also significantly influence the electronic properties of the surface as well as the corresponding adsorption and diffusion energies as we showed in Figure 10. As such, the CO coverages will also change the vibrational frequencies for the adsorbed CO. The results that are shown in Figure 12 indicate that higher CO coverages shift ν(CO) to

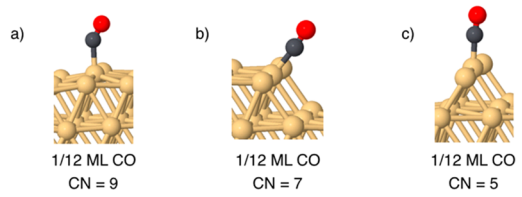

	v(CO) (cm^{-1})					
Au Site CN	1/12 ML	CO Charge	1/6 ML	CO Charge	1/3 ML	CO Charge
9	2061	0.00 e	2065	+0.01 e	2068	+0.01 e
7	2081	+0.02 e	2083	+0.02 e	2087	+0.03 e
5	2087	+0.03 e	2089	+0.03 e	2093	+0.04 e

Figure 12. Effects of CO coverage on the charge on bound CO, and its corresponding ν(CO) shift.

higher wavenumbers. The increase in coverage ultimately increases the positive charge on CO for CO bound to Au sites, which leads to larger ν(CO) shifts.

The pitting of the Au surface ultimately results in the formation of Au clusters on the Au(111) surface with monatomic height. To examine the influence of the size of the supported Au clusters on their properties, we examine the shift in CO vibrational frequency ν(CO) with Au cluster size. The results are reported in Figure 13. Although the ν(CO) depends on the actual shape of the cluster, the general trends in Figure 13 suggest that the ν(CO) moves to higher frequency as the CN of the adsorption site decreases. On small Au surface clusters, there are more low CN sites, which result in more positive charge on CO and higher ν(CO).

As the coordination number of the Au decreases, it is possible that multiple CO molecules can bind to the same Au site. This phenomenon of multiple CO adsorption is similar to that previously reported for CO on Ru particles.[56] As shown in Figure 14, two CO can readily bind to a single Au site when the Au CN = 3. The addition of a second CO to a Au site decreases

DOI: 10.1021/jacs.5b09052
J. Am. Chem. Soc. 2016, 138, 1518−1526

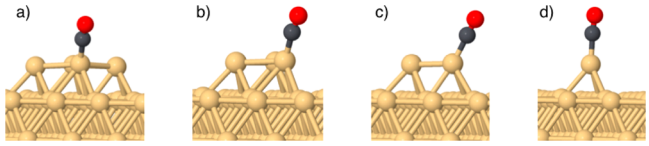

Au Particle	Cluster Size	CN	v(CO) (cm^{-1})	Charge on CO
a	4 atoms	6	2083	+0.02 e
b	3 atoms	5	2085	+0.03 e
c	2 atoms	4	2087	+0.03 e
d	1 atom	3	2094	+0.04 e

Figure 13. Effect of Au cluster size and Au coordination number on the charge on bound CO and on the ν(CO) shift.

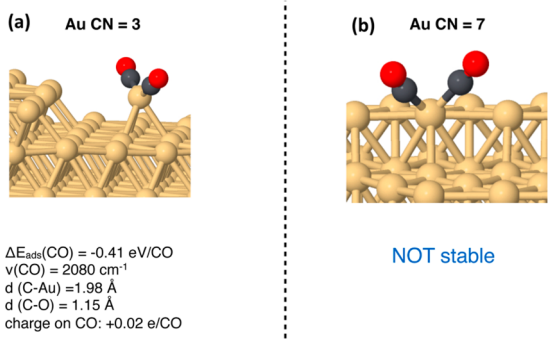

Figure 14. Multiple CO molecules on Au sites with (a) CN = 3 and (b) CN = 7.

the positive charge on each CO from +0.04 e (1 CO) to +0.02 e (2 CO), while ν(CO) shifts from 2094 cm^{-1} (1 CO) to 2080 cm^{-1} (2 CO). As such, multiple CO adsorption can also be responsible for the shift of ν(CO) to lower wavenumber for smaller Au particles or Au sites with lower coordination numbers. However, multiple CO molecules binding to a single Au center can only take place when the CN is low enough to accommodate two CO molecules. On a Au site with CN = 7, the structure with two CO molecules adsorbed on one Au atom is unstable. These two CO will automatically move to two Au sites to reach a stable structure.

The DFT results reported here provide detailed insights into the changes of electronic properties and vibrational frequencies for different Au−CO complexes at different Au sites that result during the formation, extraction, and diffusion of the Au−CO complex. Au−CO complex extraction preferentially occurs at the more coordinatively unsaturated step edge sites and the elbow sites with barriers of ~0.3 eV when these sites are highly covered with CO. These processes are thermodynamically favorable and result in CO binding to the less-coordinatively saturated site. These processes increase positive charge on CO and thus shift ν(CO) to higher wavenumbers, which is consistent with the blue-shifted wavenumbers observed in IR spectra.

IV. CONCLUSIONS

Strong evidence for the formation of Au−CO complex on Au(111) is observed for surfaces that are exposed to CO with pressures ranging from high-to-moderate vacuum by high-resolution STM and measured CO adsorption on uncoordinated Au sites by IR spectroscopy. The results were supported by DFT calculations carried out on model surfaces and clusters. Details are provided for the initial formation of the Au−CO complex at elbows of the Au(111) herringbone and low-coordinated step sites, before CO completely reconstructs the Au(111) surface. The results indicate that CO migration proceeds via a mobile Au−CO complex rather than by direct CO diffusion. The detachment of Au−CO from the low-coordinated step sites was determined to be favorable at high coverages of CO, where CO bonds to all of the low coordinated sites. These coordinatively less saturated defect sites allow for electron density to transfer from the CO to the nearby coodinatively unsaturated Au site on the Au substrate, thus altering the electronic structure of the Au sites and the potential catalytic reactivity of CO and the Au sites.

■ ASSOCIATED CONTENT

Supporting Information

The Supporting Information is available free of charge on the ACS Publications website at DOI: 10.1021/jacs.5b09052.

Results of DFT calculations on the Au_{54} cluster (PDF)

■ AUTHOR INFORMATION

Corresponding Authors

*mneurock@umn.edu

*maksymovychp@ornl.gov

Notes

The authors declare no competing financial interest.

■ ACKNOWLEDGMENTS

STM measurements were conducted at the Center for Nanophase Materials Sciences (CNMS), which is a DOE Office of Science User Facility. We thank the DOE-Office of Basic Energy Sciences under grant number DE-FGOZ-09ER16080 for partial support of this research. This work was also partially supported by the Fluid Interface Reactions, Structures and Transport (FIRST) Center, an Energy Frontier Research Center funded by the U.S. Department of Energy, Office of Science, Office of Basic Energy Science. We also thank AES Corp. for the AES Graduate Fellowship in Energy Research Program at the University of Virginia for Monica McEntee. We also gratefully thank the XSEDE computing resources from the Texas Advanced Computing Center and the San Diego Supercomputer Center for all of the DFT calculations.

■ REFERENCES

(1) Green, I. X.; Tang, W.; Neurock, M.; Yates, J. T., Jr. *Science* **2011**, *333* (6043), 736.
(2) Green, I. X.; Tang, W.; Neurock, M.; Yates, J. T., Jr. *Angew. Chem., Int. Ed.* **2011**, *50* (43), 10186.
(3) Green, I. X.; Tang, W.; McEntee, M.; Neurock, M.; Yates, J. T., Jr. *J. Am. Chem. Soc.* **2012**, *134* (30), 12717.
(4) Green, I.; McEntee, M.; Tang, W.; Neurock, M.; Yates, J. T., Jr. *Top. Catal.* **2013**, *56* (15−17), 1512.
(5) Green, I. X.; Tang, W.; Neurock, M.; Yates, J. T., Jr. *J. Am. Chem. Soc.* **2012**, *134* (33), 13569.
(6) Green, I. X.; Tang, W.; Neurock, M.; Yates, J. T., Jr. *Acc. Chem. Res.* **2014**, *47* (3), 805.
(7) McEntee, M.; Tang, W.; Neurock, M.; Yates, J. T., Jr. *J. Am. Chem. Soc.* **2014**, *136* (13), 5116.
(8) Haruta, M.; Kobayashi, T.; Sano, H.; Yamada, N. *Chem. Lett.* **1987**, *16* (2), 405.

DOI: 10.1021/jacs.5b09052
J. Am. Chem. Soc. 2016, 138, 1518−1526

(9) Hvolbæk, B.; Janssens, T. V. W.; Clausen, B. S.; Falsig, H.; Christensen, C. H.; Nørskov, J. K. *Nano Today* **2007**, *2* (4), 14 and reference therein.
(10) Kung, M. C.; Davis, R. J.; Kung, H. H. *J. Phys. Chem. C* **2007**, *111* (32), 11767.
(11) Farnesi Camellone, M.; Zhao, J.; Jin, L.; Wang, Y.; Muhler, M.; Marx, D. *Angew. Chem., Int. Ed.* **2013**, *52* (22), 5780.
(12) Rodriguez, J. A.; Ma, S.; Liu, P.; Hrbek, J.; Evans, J.; Pérez, M. *Science* **2007**, *318* (5857), 1757.
(13) Herzing, A. A.; Kiely, C. J.; Carley, A. F.; Landon, P.; Hutchings, G. J. *Science* **2008**, *321* (5894), 1331.
(14) Lopez, N.; Janssens, T. V.; Clausen, B.; Xu, Y.; Mavrikakis, M.; Bligaard, T.; Nørskov, J. *J. Catal.* **2004**, *223* (1), 232.
(15) Hammer, B. *Top. Catal.* **2006**, *37* (1), 3.
(16) Yoon, B.; Häkkinen, H.; Landman, U.; Wörz, A. S.; Antonietti, J.-M.; Abbet, S.; Judai, K.; Heiz, U. *Science* **2005**, *307* (5708), 403.
(17) Li, J.; Li, X.; Zhai, H.-J.; Wang, L.-S. *Science* **2003**, *299* (5608), 864.
(18) Wang, Y.-G.; Mei, D.; Glezakou, V.-A.; Li, J.; Rousseau, R. *Nat. Commun.* **2015**, *6*, 6511.
(19) Farnesi Camellone, M.; Kowalski, P. M.; Marx, D. *Phys. Rev. B: Condens. Matter Mater. Phys.* **2011**, *84* (3), 035413.
(20) Besenbacher, F.; Lægsgaard, E.; Stensgaard, I. *Mater. Today* **2005**, *8* (5), 26.
(21) Nielsen, L. P.; Besenbacher, F.; Laegsgaard, E.; Stensgaard, I. *Phys. Rev. B: Condens. Matter Mater. Phys.* **1991**, *44* (23), 13156.
(22) Meyer, R.; Lockemeyer, J.; Yeates, R.; Lemanski, M.; Reinalda, D.; Neurock, M. *Chem. Phys. Lett.* **2007**, *449* (1−3), 155.
(23) Łodziana, Z.; Nørskov, J. K. *J. Chem. Phys.* **2001**, *115* (24), 11261.
(24) Maksymovych, P.; Sorescu, D. C.; Yates, J. T., Jr. *Phys. Rev. Lett.* **2006**, *97* (14), 146103.
(25) Parkinson, G. S.; Novotny, Z.; Argentero, G.; Schmid, M.; Pavelec, J.; Kosak, R.; Blaha, P.; Diebold, U. *Nat. Mater.* **2013**, *12* (8), 724.
(26) Ouyang, R.; Liu, J.-X.; Li, W.-X. *J. Am. Chem. Soc.* **2013**, *135* (5), 1760.
(27) Wang, Y.-G.; Yoon, Y.; Glezakou, V.-A.; Li, J.; Rousseau, R. *J. Am. Chem. Soc.* **2013**, *135* (29), 10673.
(28) Peters, K. .; Steadman, P.; Isern, H.; Alvarez, J.; Ferrer, S. *Surf. Sci.* **2000**, *467* (1−3), 10.
(29) Piccolo, L.; Loffreda, D.; Cadete Santos Aires, F. J.; Deranlot, C.; Jugnet, Y.; Sautet, P.; Bertolini, J. C. *Surf. Sci.* **2004**, *566−568* (Part 2 (0)), 995.
(30) Jugnet, Y.; Cadete Santos Aires, F. J.; Deranlot, C.; Piccolo, L.; Bertolini, J. C. *Surf. Sci.* **2002**, *521* (1−2), L639.
(31) Loffreda, D.; Piccolo, L.; Sautet, P. *Phys. Rev. B: Condens. Matter Mater. Phys.* **2005**, *71* (11), 113414.
(32) Raskó, J.; Kiss, J. *Catal. Lett.* **2006**, *111* (1−2), 87.
(33) Diemant, T.; Zhao, Z.; Rauscher, H.; Bansmann, J.; Behm, R. J. *Top. Catal.* **2007**, *44* (1−2), 83.
(34) Hrbek, J.; Hoffmann, F. M.; Park, J. B.; Liu, P.; Stacchiola, D.; Hoo, Y. S.; Ma, S.; Nambu, A.; Rodriguez, J. A.; White, M. G. *J. Am. Chem. Soc.* **2008**, *130* (51), 17272.
(35) Pászti, Z.; Hakkel, O.; Keszthelyi, T.; Berkó, A.; Balázs, N.; Bakó, I.; Guczi, L. *Langmuir* **2010**, *26* (21), 16312.
(36) Maksymovych, P.; Yates, J. T., Jr. *Chem. Phys. Lett.* **2006**, *421* (4−6), 473.
(37) Zanella, R.; Giorgio, S.; Henry, C. R.; Louis, C. *J. Phys. Chem. B* **2002**, *106* (31), 7634.
(38) Zanella, R.; Sandoval, A.; Santiago, P.; Basiuk, V. A.; Saniger, J. M. *J. Phys. Chem. B* **2006**, *110* (17), 8559.
(39) Kresse, G. *Phys. Rev. B: Condens. Matter Mater. Phys.* **2000**, *62* (12), 8295.
(40) Kresse, G.; Joubert, D. *Phys. Rev. B: Condens. Matter Mater. Phys.* **1999**, *59* (3), 1758.
(41) Blöchl, P. E. *Phys. Rev. B: Condens. Matter Mater. Phys.* **1994**, *50* (24), 17953.
(42) Hammer, B.; Hansen, L. B.; Nørskov, J. K. *Phys. Rev. B: Condens. Matter Mater. Phys.* **1999**, *59* (11), 7413.
(43) Monkhorst, H. J.; Pack, J. D. *Phys. Rev. B* **1976**, *13* (12), 5188.
(44) Bader, R. F. *Atoms in Molecules: A Quantum Theory*; Oxford University Press: New York, 1990.
(45) Tang, W.; Sanville, E.; Henkelman, G. *J. Phys.: Condens. Matter* **2009**, *21* (8), 084204.
(46) Mavrikakis, M.; Stoltze, P.; Nørskov, J. K. *Catal. Lett.* **2000**, *64* (2−4), 101.
(47) Kim, J.; Samano, E.; Koel, B. E. *J. Phys. Chem. B* **2006**, *110* (35), 17512.
(48) Nakamura, I.; Takahashi, A.; Fujitani, T. *Catal. Lett.* **2009**, *129* (3−4), 400.
(49) Ruggiero, C.; Hollins, P. *Surf. Sci.* **1997**, *377−379* (0), 583.
(50) Yim, W.-L.; Nowitzki, T.; Necke, M.; Schnars, H.; Nickut, P.; Biener, J.; Biener, M. M.; Zielasek, V.; Al-Shamery, K.; Klüner, T.; Bäumer, M. *J. Phys. Chem. C* **2007**, *111* (1), 445.
(51) Kleis, J.; Greeley, J.; Romero, N. A.; Morozov, V. A.; Falsig, H.; Larsen, A. H.; Lu, J.; Mortensen, J. J.; Dułak, M.; Thygesen, K. S.; Nørskov, J. K.; Jacobsen, K. W. *Catal. Lett.* **2011**, *141* (8), 1067.
(52) Janssens, T. W.; Clausen, B.; Hvolbæk, B.; Falsig, H.; Christensen, C.; Bligaard, T.; Nørskov, J. *Top. Catal.* **2007**, *44* (1−2), 15.
(53) Zeng, Z.; Greeley, J. *Catal. Commun.* **2014**, *52*, 78.
(54) Liu, Z.-P.; Hu, P.; Alavi, A. *J. Am. Chem. Soc.* **2002**, *124* (49), 14770.
(55) Hussain, A.; Curulla Ferré, D.; Gracia, J.; Nieuwenhuys, B. E.; Niemantsverdriet, J. W. *Surf. Sci.* **2009**, *603* (17), 2734.
(56) Loveless, B. T.; Buda, C.; Neurock, M.; Iglesia, E. *J. Am. Chem. Soc.* **2013**, *135* (16), 6107.

DOI: 10.1021/jacs.5b09052
J. Am. Chem. Soc. 2016, 138, 1518−1526